CHAPTER-3

Human Locomotion Classification for Different Terrains using Machine Learning Techniques

Highlights of the Chapter

- *This chapter presents the EMG and acceleration signal-based terrain classification*
- *Five conventional machine learning classifiers and deep neural network classifiers were used*
- *In terms of accuracy and time, the support vector machine showed remarkable performance compared to other classifiers*

ABSTRACT

Purpose – This chapter presents human locomotion classification by implementing machine learning techniques on surface electromyographic and acceleration sensor data collected from healthy subjects.

Design/methodology/approach – Five terrains were chosen to acquire the surface electromyography (sEMG) and 3-axes acceleration signals: level ground, ramp ascent, ramp descent, stair ascent, and stair descent. The signals were acquired from the tibialis anterior and gastrocnemius medial head muscles corresponding to dorsiflexion and plantarflexion. Once the signal acquisition was completed, various feature extraction techniques were applied. Subsequently, the processed data was fed into the following classifiers: linear discriminant analysis (LDA), k-nearest neighbors (KNN), decision tree (DT), random forest (RF), and support vector machine (SVM) to classify different terrains. The results from the above classifiers were compared with the results obtained from a deep neural network (DNN) classifier. The present work analyzes conventional machine learning techniques and deep neural networks on data obtained from two leg

muscles while walking on various terrains. The primary focus is to maximize classification accuracy and minimize prediction time.

Findings – The scatter plots are obtained using filtered EMG data, and the feature set provided the best discrimination among five locomotion modes with maximum classification accuracy. From the results, it is inferred that the SVM gave the highest accuracy of 99.20 (± 0.80) % while outperforming other classifiers.

Practical implications – This study might help design a real-time control mechanism for an ankle-foot prosthetic device capable of supporting various locomotion modes.

Originality/value – The surface EMG and acceleration signals are acquired from the TA and MGAS muscles for five terrains. After filtering and feature extraction, different ML techniques were investigated for terrain classification, and the results were compared for different classifiers.

3.1 Introduction

Gait analysis is a systematic and quantitative study performed to assess the intricacies of human locomotion (Winter 1991). Common approaches to analyzing the gait phase include vision-based methods, sensor-based methods, and sometimes hybrid methods. These systems are available in both wearable and non-wearable forms. Vision-based gait analysis is performed using non-wearable devices; however, these are restrained to the laboratory surroundings. Gait recognition using wearable sensing devices is an active studies region in gait analysis. Wearable sensing systems utilizing accelerometers, gyroscope, goniometer, force sensor, and electromyography (EMG) have been utilized by many researchers (Tao et al., 2012; Prakash et al., 2018). Those methods can be divided into gait kinematics, gait kinetics, and electromyography. The kinematics of the human gait defines the activity of the principal joints and additives within the lower limbs.

It highlights the study of forces and moments that causes the movements of human segments.

During walking, the following mechanical function occurs: momentum for forwarding progression, foot position control, energy absorption, forward acceleration of the limb, and deceleration of the limb, where the first two functions are performed by the ankle muscles (Yang et al., 1985). Depending on these mechanical functions, the EMG signal acquired from different muscles has a pattern that may be used as input to the classifiers to classify human locomotion modes. Therefore, the knowledge of the muscles responsible for the movement of the ankle-foot and the user's movement intent is necessary while designing an artificial ankle-foot so that proper control mode can be selected to adjust the ankle joint impedance. Patla (1985) monitored the myoelectric signals from tibialis anterior (TA), soleus (SO), medial gastrocnemius (MGAS), vastus lateralis (VA), rectus femoris (RF), biceps femoris (BF), and erector spinae (ES) muscles of ipsilateral limb for treadmill walking for varying stride lengths and speeds. The muscles mentioned above act as an extensor and flexor for the three joints of the lower limb. Dorsiflexion is characterized by the proximity of toes to shin and reduction of the angle between leg and foot dorsum. Plantarflexion is characterized by reducing the angle between the back of the leg and the sole (Winter 1991).

As stated earlier, gait analysis can be carried out by implementing a variety of methods. (Huang et al. 2008), detected gait events using a force-sensitive resistor (FSR)-based footswitches placed beneath the foot and reflective markers placed on heel and toe. The MA-300-16 system was used to acquire 16 channel EMG data and footswitch data simultaneously. To capture the position of reflective markers, six motion capture cameras were used. An algorithm to continuously recognize different locomotion modes in transfemoral (TF) amputees was developed by (Huang et al., 2011). This algorithm is

based on a combination of mechanical and EMG signals. For upper-limb prostheses, myoelectric pattern recognition-based control is widely used. For lower limb applications, however, there is somewhat limited research (Zhang et al., 2012; Liu et al., 2017). A major portion of research in lower limb prostheses involves TF amputees. For transtibial (TT) amputees, the number of publications is still small. There remains potential for research in controlling ankle-foot prostheses based on intent recognition (Chen et al., 2013). The fundamental principle of myoelectric-based prosthetics is detecting electrical signals from residual nerves of amputees (Kumar et al., 2017). The main reason why the ankle joint is of utmost importance in ankle prostheses design is that it receives the whole weight of the body. The motivation behind the current study is a thorough analysis of the gait phase to design a low-cost powered below-knee (or ankle-foot) prosthesis.

Knowledge of an optimum pattern recognition algorithm is essential to ensure proper control of ankle-foot prostheses. Before feeding the data into the classifier, the data undergoes pre-processing. This step involves the extraction of features, be it time-domain or frequency-mode. Mainly this is achieved by using the windowing technique (Phinyomark et al., 2012; Negi et al., 2016; Gupta et al., 2018). Time-frequency delineation of EMG was used to classify locomotion modes by Joshi et al. (2015) through the implementation of simple if-else rules. When the volume of data is high, often, feature extraction is performed to reduce the dimensionality of the data. Standard dimensionality reduction techniques are principal component analysis (PCA), linear discriminant analysis (LDA), and uncorrelated linear discriminant analysis (ULDA) for dimensionality reduction (Chan et al., 2007). Ivanenko et al. (2004) applied PCA to a normalized EMG pattern over a step cycle. To improve classification accuracy, an iterative greedy selection-based feature selection algorithm was proposed by Gupta et al. (2018) for multi

muscle-based locomotion identification. Various machine learning (ML) methods can segregate the locomotion mode generating ~~a~~ control signal for prosthetic devices.

This chapter aims to investigate different ML techniques for terrain classification. In present work, six classifiers are implemented: (i) linear discriminant analysis (LDA), (ii) k-nearest neighbors (KNN), (iii) decision tree (DT), (iv) random forest (RF), (v) support vector machine (SVM) and (vi) deep neural network (DNN). The primary focus of the current study is to find the classifier that achieves maximum accuracy in the shortest time.

3.2 Implementation of Machine Learning Techniques for Gait Analysis

The branch of artificial intelligence which deals with the learning and development of intelligent systems is called ML. In ML, a machine or a system is tasked to learn from data and make decisions with minimal human involvement (Raschka 2015; Prakash et al. 2018). Broadly, the ML techniques are subdivided into supervised, unsupervised, semi-supervised, and reinforcement learning. In supervised learning, the model is trained from labeled data and is tested for prediction accuracy with unknown/unseen data. One of the major applications of supervised learning is the classification problem, i.e., predicting the class labels for the data (Raschka 2015). Unsupervised algorithms do not have class labels. These models aim to group the data based on similarity (Garreta et al., 2013). Semi-supervised learning involves a small portion of labeled data and a large volume of unlabelled data. Reinforcement learning works on a penalty/reward system, where correct prediction rewards the model while a wrong prediction penalizes the model (Géron, 2019).

To tackle human locomotion identification-related problems, mostly supervised algorithms are used. All the scripts used in the current study were written in Python and involved using various libraries like scikit-learn and TensorFlow to perform operations

(Team, P.C. 2015; Pedregosa et al., 2011; Abadi et al., 2016). **S**everal classification methods used in such tasks are LDA (Huang et al., 2008; Chen et al., 2013; Gupta et al., 2018), SVM (Gupta et al., 2018; Huang et al., 2011), KNN, neural network (N.N.) (Gupta et al., 2018; Huang et al., 2008), D.T., R.F., correlation feature analysis (Kim 2014), entropy-based adaptation (EBA) (Liu et al., 2017).

3.3 Materials and Methods

3.3.1 Data Collection

In the present study, 15 able-bodied subjects (ten male and five female) were included with proper consent and approval from the subjects and the ethical committee of the Institute of Medical Sciences, BHU, Varanasi. The mean (± std) age, weight, and height of healthy subjects are 22 (± 8.4) years, 62 (± 13.9) kg, and 166 (± 8.3) cm, respectively. To acquire EMG and 3-axes acceleration signals, Delsys Trigno wireless setup was used. The EMG and acceleration data obtained from TA and MGAS muscles is shown in Figure 3.1. As stated above, the sensors are placed on TA and MGAS muscles of the lower limb as these muscles are involved in dorsiflexion and plantar flexion of the foot, respectively. De Luca (2002 and 2006) highlighted the fundamentals of EMG recording and detailed specifications of the EMG sensors. The five terrains considered for this study are level ground (LG), ramp ascent (RA), ramp descent (RD), stair ascent (SA), and stair descent (SD), with each subject performing ten trials of 5 seconds each for every terrain. The sampling rate of the EMG signals was 1926 samples/sec and 148 samples/sec for acceleration signals. Both signals were resampled at 1000 samples/sec using EMGworks software on a computer. The computer specifications are an 8^{th} generation i7 processor (2.50GHz), 16GB RAM, and 8 GB NVIDIA Quadro P4000 GPU.

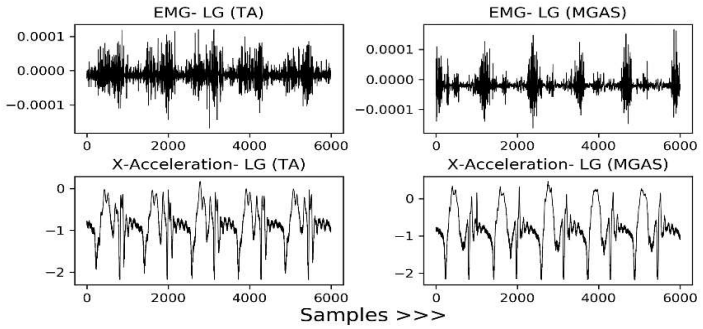
EMG- LG (TA)
EMG- LG (MGAS)
X-Acceleration- LG (TA)
X-Acceleration- LG (MGAS)
Samples >>>

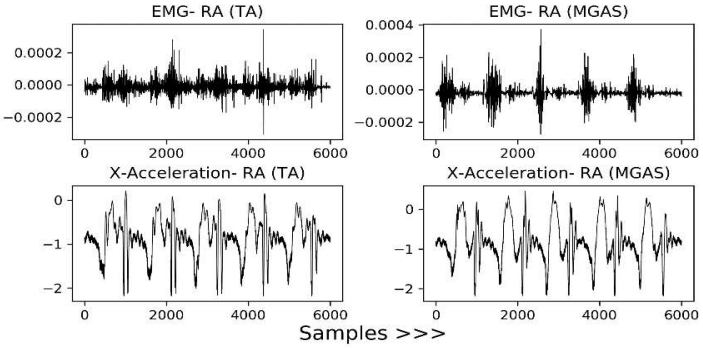
EMG- RA (TA)
EMG- RA (MGAS)
X-Acceleration- RA (TA)
X-Acceleration- RA (MGAS)
Samples >>>

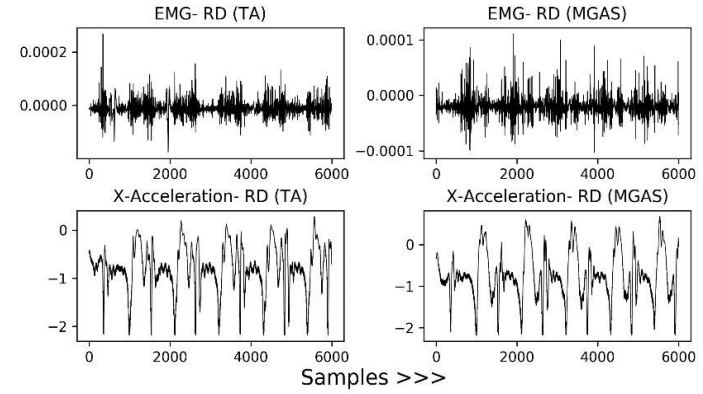
EMG- RD (TA)
EMG- RD (MGAS)
X-Acceleration- RD (TA)
X-Acceleration- RD (MGAS)
Samples >>>

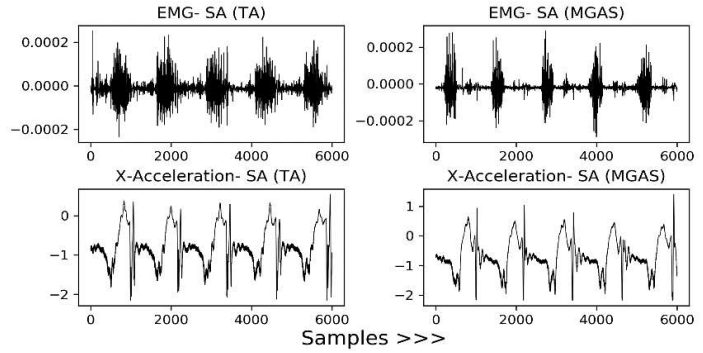
EMG- SA (TA)
EMG- SA (MGAS)
X-Acceleration- SA (TA)
X-Acceleration- SA (MGAS)
Samples >>>

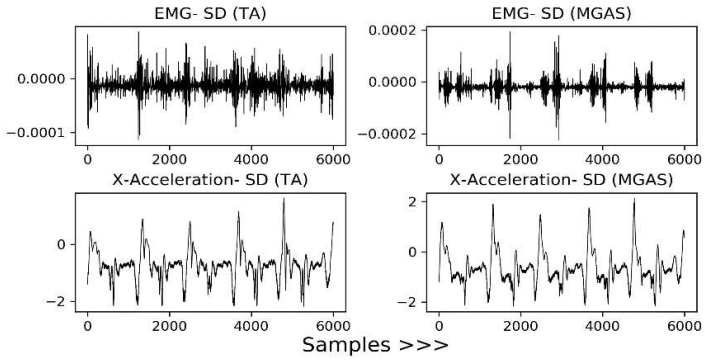

Figure 3.1 *EMG and X- Acceleration signals acquired from right leg TA and MGAS muscles for five different terrain walks*

3.3.2 Data Analysis

Further processing of the acquired signals includes multiple steps like filtering, feature extraction, normalization, and feature vector preparation. For EMG signals, the filtering was done using bandpass filters at 20-450Hz, and for acceleration signals, the filtering was done using a low pass filter at 10Hz. The filtered data was then stored in vectors, and feature extraction was carried out using various python libraries like NumPy, pandas, and matplotlib (Van Der Walt et al., 2011; Hunter, 2007). The standardization of the data was done using scikit-learn. The processed data was split into training and testing datasets and fed into conventional classifiers coded using scikit-learn and the neural network coded using tensorflow. (Pedregosa et al., 2011, Abadi et al., 2016).

3.3.3 Machine Learning-based Predictive Model

The complete workflow of the present study is shown in Figure 3.2. First, the acquired data is pre-processed. In the pre-processing step, the data was synchronized in the same time frame, filtered, scaled, and finally, feature extraction was carried out. The data is then split into training and testing sets. The model is trained using the training dataset, while the testing dataset is used to evaluate the model's performance. Another unseen dataset that was not part of training was used to test the model's prediction accuracy.

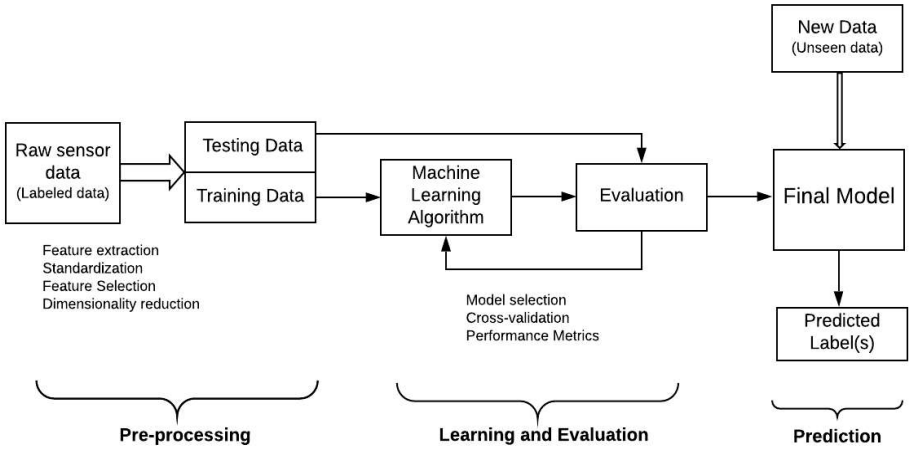

Figure 3.2 *Workflow diagram of machine learning-based predictive modelling*

Below is the summarized algorithm for the present study:

Algorithm 3.1: *Machine learning-based prediction*

1. Acquisition of sEMG and acceleration signals. Signals have been acquired from TA and MGAS muscles for five locomotion modes using Delsys Trigno wireless setup.
2. Labeling of data for training.
3. Feature selection: (i) Computation of features, (ii) Evaluation of features and feature vectors.
4. Training of LDA, KNN, DT, RF, SVM, and DNN classifiers.
5. K-fold validation of the classifier model.
6. Classification of unseen data using trained classifier model.

3.3.4 Feature Selection

The process of gaining valuable insights from the data and eliminating unwanted features is called feature extraction. In order to analyze gait signals, researchers frequently use statistical or spectral, or wavelet features (Phinyomark et al., 2012; Negi et al., 2016; Gupta et al., 2018). In the present study, following statistical features are used (i) root mean square (RMS), (ii) integrated absolute value (IAV), (iii) mean absolute value (MAV), (iv) modified mean absolute value (MAV1), (v) waveform length (WL), (vi) mean, (vii) standard deviation (SD), (viii) maximum, (ix) minimum, (x) simple square

integral (SSI), (xi) variance, (xii) 3rd, 4th and 5th temporal moments, (xiii) average amplitude change (AAC), (xiv) difference absolute standard deviation value (DASDV), (xv) zero-crossing (ZC), (xvi) slope sign change (SSC), (xvii) kurtosis, (xviii) skewness, (xix) Willison amplitude (WL) and (xx) myopulse percentage rate. The mathematical expressions of some of the features are shown below from Equations 3.1 to 3.8. The separability of classes was assessed using a scatterplot of individual features as mentioned in (Phinyomark et al., 2012; Negi et al., 2016). It was observed that the combination of features in Equations 3.1, 3.2, 3.4, and 3.5 showed the highest separability of the classes. Mathematical expression for Root Mean Square (RMS):

$$RMS = \sqrt{\frac{1}{N}\sum_{i=1}^{N} x_i^2} \tag{3.1}$$

where,

x_i = EMG signal in a segment i

N = length of the EMG signal

Expression for Integrated Absolute Value (IAV):

$$IAV = \sum_{i=1}^{N} |x_i| \tag{3.2}$$

Mean Absolute Value (MAV): MAV is an average of the absolute value of the EMG signal amplitude in a segment, expressed by

$$MAV = \frac{1}{N}\sum_{i=1}^{N} |x_i| \tag{3.3}$$

Modified Mean Absolute Value type 1 (MAV1): MAV1 is an extension of the MAV feature. Here a weighted window function w_i is added to improve the robustness of the MAV feature. It is calculated as

$$MAV1 = \frac{1}{N}\sum_{i=1}^{N} w_i|x_i|; \quad 3.4$$

where $w_i = \begin{cases} 1 & if\ 0.25N \le i \le 0.75N \\ 0.5 & otherwise \end{cases}$

Waveform Length (WL): WL is the cumulative length of the EMG waveform over the time segment and is defined as

$$WL = \sum_{i=1}^{N-1} |x_{i+1} - x_i| \quad 3.5$$

Simple Square Integral (SSI): This is also called Integral square. SSI uses the energy of the EMG signal as a feature. It is a summation of square values of the EMG signal amplitude.

$$SSI = \sum_{i=1}^{N} x_i^2 \quad 3.6$$

Variance (VAR): The variance (or second-order moment) of the EMG signal is a measure of the signal power and is calculated as

$$VAR = \frac{1}{N-1}\sum_{i=1}^{N} x_i^2 \quad 3.7$$

The 3rd, 4th, and 5th temporal moments: The 3rd, 4th, and 5th order moments (TM3, TM4, and TM5) can be expressed as

$$TM3 = \frac{1}{N}\sum_{i=1}^{N} x_i^3; \qquad TM4 = \frac{1}{N}\sum_{i=1}^{N} x_i^4; \qquad TM5 = \frac{1}{N}\sum_{i=1}^{N} x_i^5 \quad 3.8$$

3.4 Results and Discussion

Fifteen subjects' data is acquired from two muscles (TA/MGAS) for five different terrains - LG, RA, RD, SA, and SD. Figure 3.3 shows the envelope of EMG signals acquired from TA and MGAS muscles of subject-15 for all-terrain. It also indicates that the gait events heel-strike, toe-off, and mid-swing were correctly detected using an acceleration signal (Negi et al., 2020). One can examine from Figure 3.3 that contraction and relaxation of both muscles are related to the locomotion patterns and could therefore supply

information for the identification of terrain. Many time-domain features presented in (Phinyomark et al., 2012; Negi et al., 2016; Gupta et al., 2018) were evaluated in the current study.

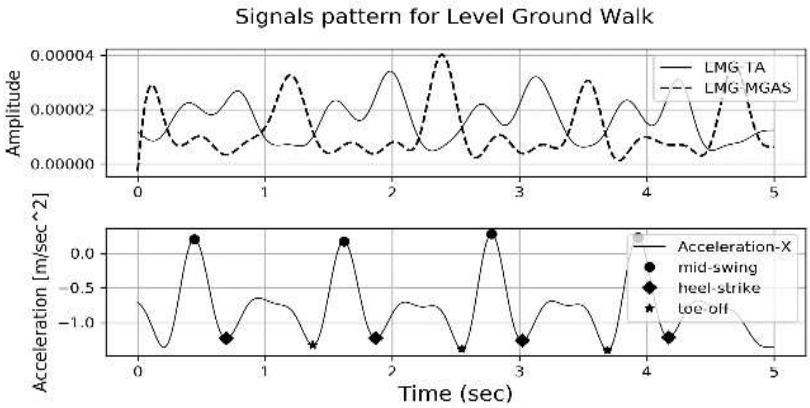

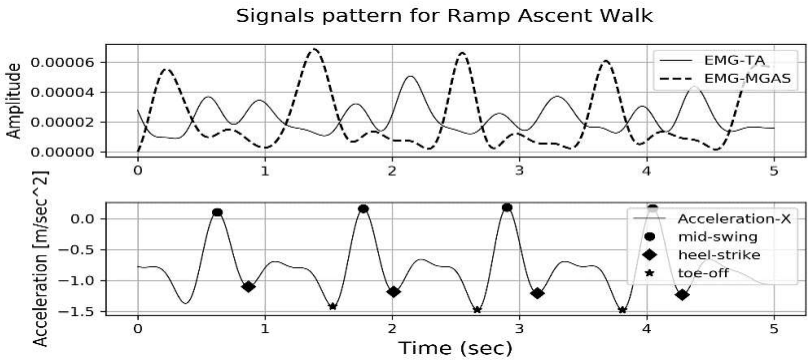

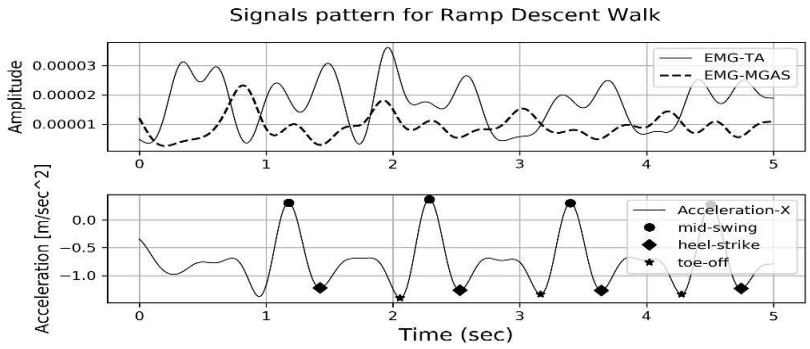

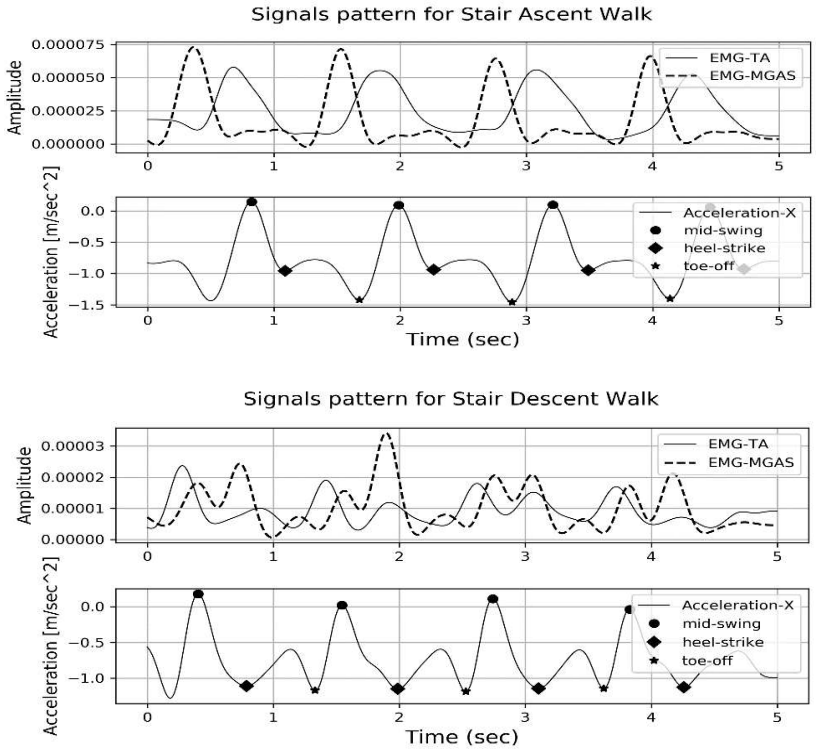

Figure 3.3 *EMG-envelope for different terrains and corresponding Gait events detected using acceleration signal*

The scatter plots between two EMG channels (i.e., TA and MGAS muscles) were checked for different features, and it was found that for filtered EMG data, feature set [RMS, IAV, W.L., MAV1] provided the best discrimination among five locomotion modes with maximum classification accuracy. The scatter plot for these selected features is shown in Figure 3.4. Also, it can be easily seen from the scatter plots that for three terrains classification problems (i.e., LG, SA, and SD), the classes are easily separable using a simple decision boundary, whereas as the classes increase up to 5 (i.e., for LG, RA, RD, SA, and SD), one needs such a classifier that can separate these complex boundaries.

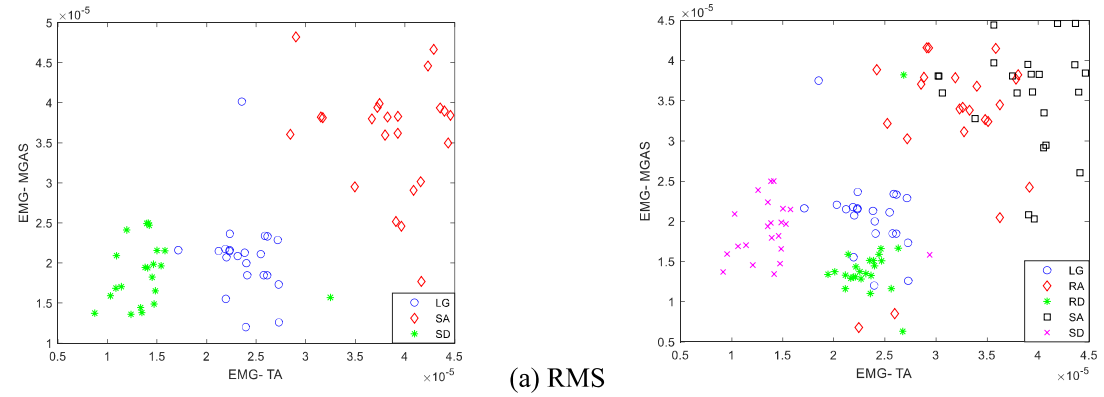

(a) RMS

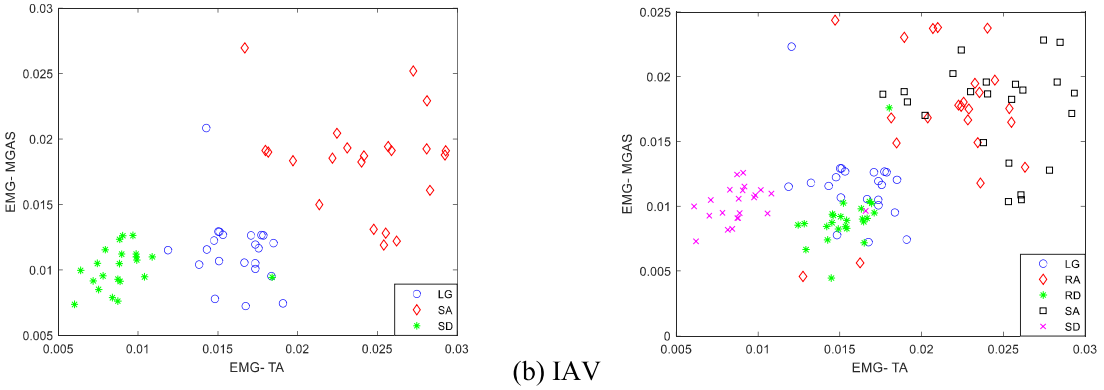

(b) IAV

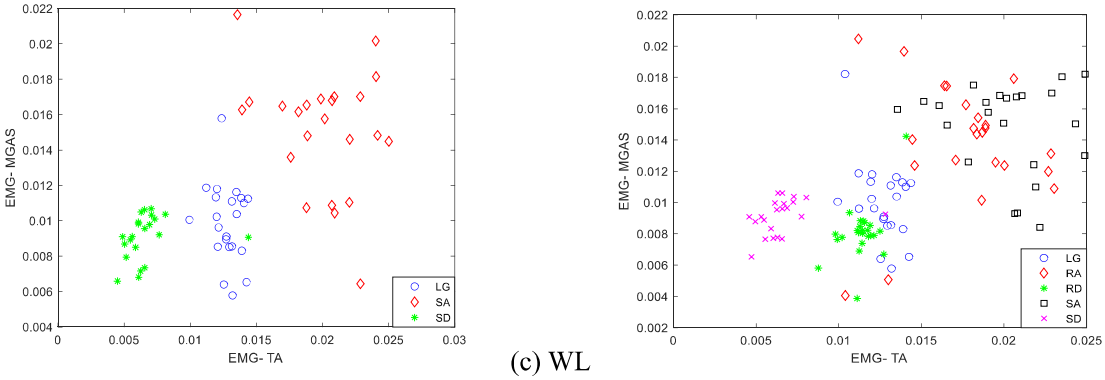

(c) WL

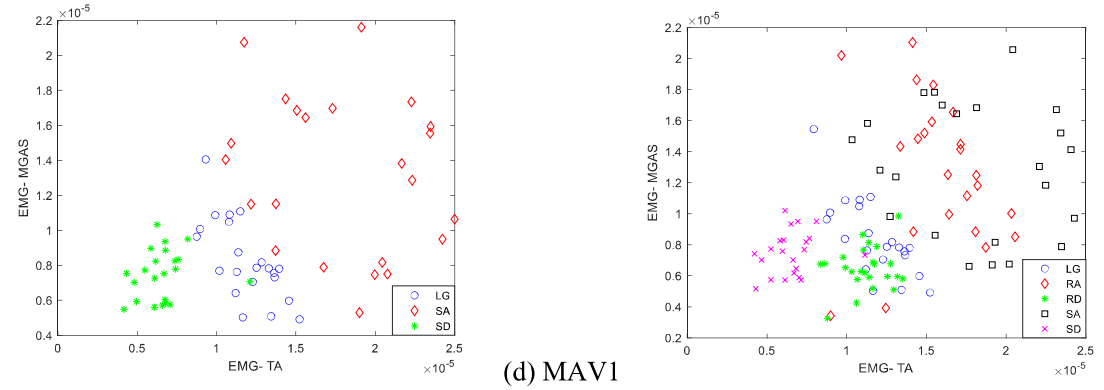

(d) MAV1

Figure 3.4 *Scatter plot for EMG data from two muscles for (a) RMS, (b) IAV, (c) WL, and (d) MAV1 features*

The sliding window technique is used for feature extraction, where various window sizes and window increment values are selected. We obtained the results for different combinations of these and presented the results for winsize/wininc = 256/32, 256/16, 512/64, and 512/32, where winsize represents the size of the window (in samples), and wininc represents the samples by which the window is incremented.

The dataset consists of 10-trials data for each subject for five terrains. 80% of data is selected for training from the known dataset, and the remaining 20% is used for testing. Tables 3.1 to 3.8 display the classification accuracy obtained for the LDA, KNN, DT, RF, SVM, and DNN classifiers. For the validation of results, 10-fold cross-validation was used for all conventional classifiers. In the case of the DNN classifier, we calculated the accuracy first by using feature extraction and later without using feature extraction.

Table 3.1 *Classification accuracy of LDA classifier*

winsize/wininc	Classification accuracy (%) [mean ± std]	Cross-validation score
512/64	89.85 (± 4.95)	0.885 (± 0.051)
512/32	90.62 (± 4.76)	0.885 (± 0.052)
256/32	73.01 (± 6.84)	0.718 (± 0.071)
256/16	73.56 (± 6.60)	0.718 (± 0.071)

Table 3.2 *Classification accuracy of KNN classifier*

K	winsize/wininc	Classification accuracy (%) [mean ± std]	Cross-validation score
2	512/64	91.87 (± 4.59)	0.747 (± 0.097)
2	512/32	97.21 (± 1.95)	0.782 (± 0.088)
2	256/32	87.40 (± 5.43)	0.685 (± 0.103)
2	256/16	95.70 (± 1.98)	0.725 (± 0.097)
4	512/64	92.03 (± 4.78)	0.759 (± 0.096)
4	512/32	96.72 (± 2.22)	0.785 (± 0.088)
4	256/32	88.51 (± 5.33)	0.697 (± 0.106)

4	256/16	94.86 (± 2.70)	0.727 (± 0.099)
6	512/64	91.77 (± 4.82)	0.761 (± 0.096)
6	512/32	96.33 (± 2.33)	0.786 (± 0.088)
6	256/32	88.11 (± 5.72)	0.697 (± 0.108)
6	256/16	94.00 (± 3.24)	0.730 (± 0.100)

Table 3.3 *Classification accuracy of DT classifier*

winsize/wininc	Classification accuracy (%) [mean ± std]	Cross-validation score
512/64	91.09 (± 3.64)	0.664 (± 0.073)
512/32	95.42 (± 1.83)	0.667 (± 0.071)
256/32	88.85 (± 3.52)	0.644 (± 0.075)
256/16	93.75 (± 2.04)	0.654 (± 0.077)

Table 3.4 *Classification accuracy of RF classifier*

winsize/wininc	Classification accuracy (%) [mean ± std]	Cross-validation score
512/64	95.32 (± 2.85)	0.690 (± 0.108)
512/32	98.63 (± 0.84)	0.703 (± 0.105)
256/32	93.51 (± 3.64)	0.650 (± 0.116)
256/16	98.16 (± 1.35)	0.673 (± 0.115)

Table 3.5 *Classification accuracy of SVM (RBF-kernel) classifier*

winsize/wininc	Classification accuracy (%) [mean ± std]	Cross-validation score
512/64	97.68 (± 1.73)	0.939 (± 0.040)
512/32	99.20 (± 0.80)	0.942 (± 0.039)
256/32	96.10 (± 2.40)	0.917 (± 0.048)
256/16	98.01 (± 1.57)	0.923 (± 0.047)

Table 3.6 *Classification accuracy of SVM (Poly-kernel) classifier*

winsize/wininc	Classification accuracy (%) [mean ± std]	Cross-validation score
512/64	97.57 (± 1.63)	0.924 (± 0.048)
512/32	99.31 (± 0.55)	0.928 (± 0.047)
256/32	96.34 (± 2.31)	0.901 (± 0.053)
256/16	98.59 (± 1.35)	0.904 (± 0.053)

Table 3.7 *Classification accuracy of DNN classifier [with feature extraction]*

winsize/wininc	Classification accuracy (%) [mean ± std]	Precision	Recall	F1 score
512/64	97.12 (± 1.52)	0.971 (± 0.015)	0.971 (±0.015)	0.971 (± 0.015)
512/32	99.02 (± 0.86)	0.990 (± 0.009)	0.990 (± 0.009)	0.990 (± 0.009)
256/32	95.52 (± 2.73)	0.956 (± 0.026)	0.954 (± 0.028)	0.955 (± 0.027)
256/16	98.72 (± 0.88)	0.987 (± 0.009)	0.987 (± 0.009)	0.987 (± 0.009)

Table 3.8 *Classification accuracy of DNN classifier [without feature extraction]*

Classification accuracy (%) [mean ± std]	Precision	Recall	F1 score
98.53 (± 0.42)	0.986 (± 0.004)	0.985 (±0.004)	0.985 (± 0.004)

The maximum accuracy observed for all classifiers was for window size and window increment of 512 and 32, respectively. The plot for errors on various k values is shown in Figure 3.5, and minimum error was observed at k=2 for the KNN classifier. For the KNN classifier, we obtained the readings for even k (i.e., k = 2, 4, and 6), as we have an odd number of classes (i.e., 5). From Tables 3.1 to 3.8 it can be observed that the classification accuracy of over 97% was achieved by SVM and DNN.

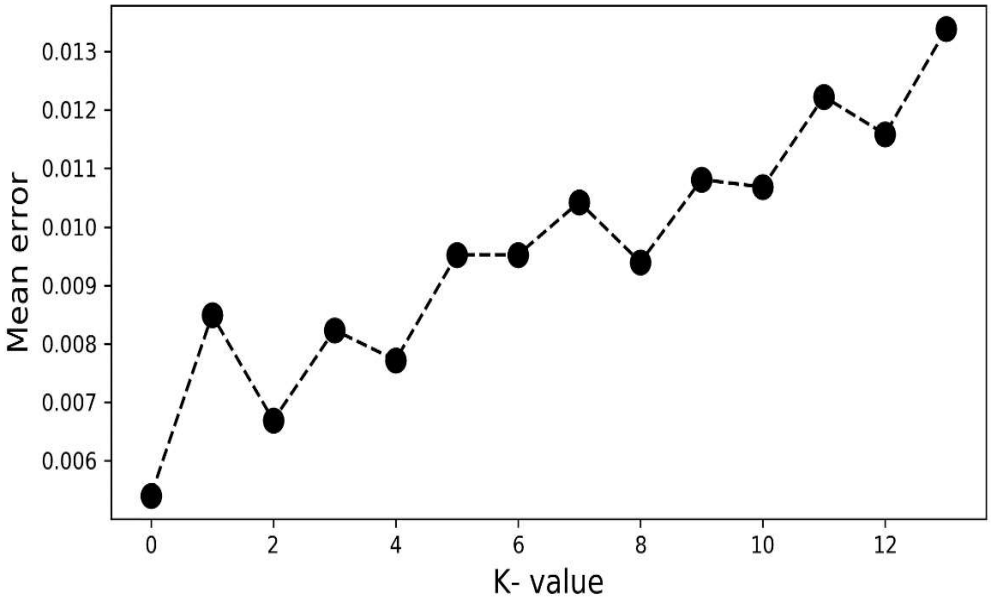

Figure 3.5 *Error Rate vs. K- values*

An important metric to consider is the time taken to predict unseen data to select the best classifier. The comparison of accuracy and computation time for every classifier is summarised in Table 3.9. For this, the classifiers were trained with 10- trial data of each class for Subject-03. The testing was done on a different dataset of the same subject. Although LDA, DT, and RF provide the optimal performance, they take a long time in computation and give low scores in cross-validation.

Although DNN showed excellent accuracy for the data, it suffered from a long computation time compared to other classifiers. For DNN, various model architectures were trained and tested for performance. For the hidden layer, Rectified linear units (ReLU) activation function is used. For the output layer, the Softmax function is used.

Table 3.9 *Comparison of classification accuracy and evaluation time of classifiers for the testing of single trial data of each class*

Classifier	winsize/ wininc 512/64		winsize/ wininc 512/32		winsize/ wininc 256/32		winsize/ wininc 256/16	
	Accuracy	Time	Accuracy	Time	Accuracy	Time	Accuracy	Time
KNN (K=2)	97.71 %	0.42 sec	97.57 %	0.65 sec	94.86 %	0.63 sec	95.74 %	1.12 sec
LDA	96.86 %	0.32 sec	96.71 %	0.40 sec	85.13 %	0.40 sec	85.27 %	0.57 sec
DT	79.71 %	0.33 sec	83.14 %	0.42 sec	74.19 %	0.40 sec	76.49 %	0.57 sec
RF	80.00 %	0.32 sec	82.29 %	0.41 sec	80.00 %	0.42 sec	77.70 %	0.58 sec
SVM (RBF-kernel)	96.86 %	0.34 sec	96.43 %	0.48 sec	96.49 %	0.50 sec	96.35 %	0.87 sec
SVM (Poly-kernel)	98.85 %	0.34 sec	97.71 %	0.44 sec	94.59 %	0.44 sec	93.72 %	0.67 sec
DNN (with feature extraction)	96.00 %	1.38 sec	95.57 %	1.84 sec	95.81 %	1.53 sec	96.55 %	1.64 sec
DNN (without feature extraction)	80.66%	2.88 sec						

In Tables 3.7 and 3.8, the DNN results are shown for the input layer of size-8, seven hidden layers of size-32, 128, 512, 512, 128, 32, 8, and the output layer of size-5. The results of DNN are represented using a confusion matrix. In Figure 3.6 (a), the confusion matrix is shown for the training dataset. Figure 3.6 (b) shows the confusion matrix for the single-trial unseen dataset.

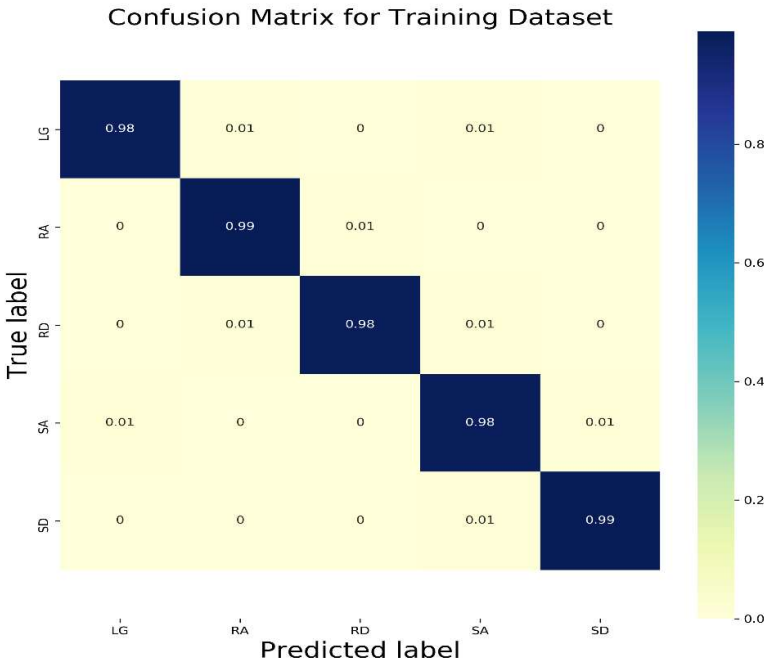

(a)

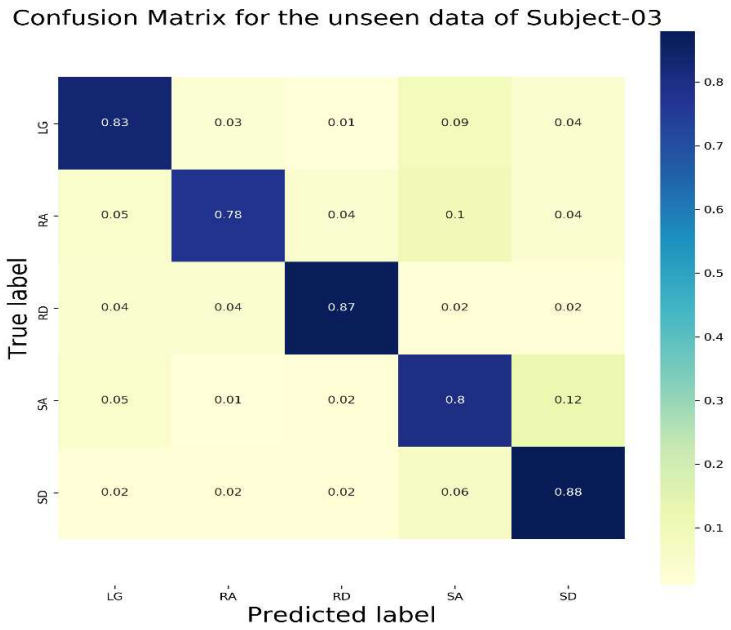

(b)

Figure 3.6 *Confusion matrix of DNN classifier for Subject-03 (a) 10-trials training dataset, (b) unseen data.*

3.5 Conclusion

In this chapter, the EMG and acceleration signal-based terrain classification for two leg muscles is presented. The classifiers used are LDA, KNN, DT, RF, SVM, and DNN. 80% of the known dataset data was used for training, and the testing was done using the remaining 20% of data. It was observed that the SVM classifier provided the highest score amongst all the classifiers. It achieved 99.20 (± 0.80) % classification accuracy and 0.942 (± 0.039) cross-validation score, and took only 0.34 sec to classify an unseen dataset of 25000 samples. Thus, it can be inferred that the SVM classifier is suitable for locomotion mode classification in a small sample size. A potential application of this study is to lay a groundwork for the design of a real-time control mechanism for an ankle-foot prosthetic device capable of supporting various locomotion modes.